CMS Physics Analysis Summary

Contact: cms-pag-conveners-ewk@cern.ch 2011/03/18

Measurement of Forward-Backward Asymmetry of Lepton Pairs and the Weak-mixing Angle at CMS

The CMS Collaboration

Abstract

We present a measurement of the forward-backward asymmetry (A_{FB}) of opposite sign lepton pairs (e^+e^- and $\mu^+\mu^-$) produced via an intermediate $Z/\gamma*$ in LHC proton-proton collisions at $\sqrt{s}$ = 7 TeV. We also present a measurement of the effective weak-mixing angle (θ_{eff}) via a multivariate likelihood fit of the rapidity, dilepton invariant mass, and decay angle distributions. Our results are based on an integrated luminosity up to 40 pb^{-1}. We present A_{FB} as a function of mass in the range $40 < M_{\ell^+\ell^-} < 600$ GeV range. From the dominant $u\bar{u}$ and $d\bar{d} \to Z/\gamma^* \to \mu^+\mu^-$ processes, we measure $\sin^2\theta_{eff} = 0.2287 \pm 0.0077 \pm 0.0036$. We find both the A_{FB} and the $\sin^2\theta_{eff}$ measurements to be consistent with the Standard Model predictions within uncertainties.

1 Introduction

In the process $q\bar{q} \to Z/\gamma^* \to \ell^+\ell^-$, both the vector and axial-vector couplings of electroweak bosons to fermions are present. This results in a forward-backward asymmetry ($A_{\rm FB}$) in the number of Drell-Yan lepton pairs. In the Standard Model, this asymmetry depends on the di-lepton invariant mass, quark flavor, and electroweak mixing angle θ_W. Deviations from the Standard Model prediction for $A_{\rm FB}$ may indicate the existence of a new neutral gauge boson [1–6], quark-lepton compositeness [7], supersymmetric particles, or extra dimensions [8]. The measurement of the forward-backward asymmetry can also improve QCD measurements with higher-order corrections and constrain Parton Distribution Functions (PDFs). The measurement of the asymmetry can provide a precise measurement of $\sin^2\theta_{\rm eff}$, the effective electroweak mixing parameter which includes a higher-order correction with respect to the tree-level couplings with $\sin^2\theta_W$. The asymmetry as a function of mass also provides information on the u and d quarks separately [9]. Initial $A_{\rm FB}$ studies in CMS using Monte Carlo (MC) events are described in references [10, 11] and the first preliminary measurement of the asymmetry in the muon channel without any corrections is documented in [12–14]. In this study, we consider the di-muon and di-electron final states. The asymmetry and $\sin^2\theta_W$ measurements by the CDF and D0 Collaborations can be found in [9, 15, 16].

In addition to the traditional asymmetry measurements discussed above, we present a multivariate analysis which uses full information about the Drell-Yan process $q\bar{q} \to Z/\gamma^* \to \ell^+\ell^-$ parameterized as a function of the di-lepton rapidity Y, di-lepton invariant mass squared s, and di-lepton decay angle θ^*_{CS} defined in the Collins-Soper frame [17]. We build the formalism based on the idea of an analytical description of the full process starting from elementary interactions through the observed objects and including a description of the detector effects, encouraged by the feasibility studies of a resonance polarization in Ref. [18].

At a given value of the di-lepton invariant mass, the differential cross-section for the parton-level process can be written as

$$\frac{d\sigma}{d\cos\theta} = A(1+\cos^2\theta) + B\cos\theta \tag{1}$$

where θ is the emission angle of the lepton relative to the quark momentum in the center-of-mass frame, and A and B are parameters that depend on the weak isospin and charge of the incoming fermions. The cross sections for the forward ($\sigma_{\rm F}$) and backward events ($\sigma_{\rm B}$) are then

$$\begin{aligned}\sigma_{\rm F} &= \int_0^1 \frac{d\sigma}{d(\cos\theta)} d(\cos\theta) = A\left(1+\frac{1}{3}\right) + B\left(\frac{1}{2}\right) \\ \sigma_{\rm B} &= \int_{-1}^0 \frac{d\sigma}{d(\cos\theta)} d(\cos\theta) = A\left(1+\frac{1}{3}\right) - B\left(\frac{1}{2}\right)\end{aligned} \tag{2}$$

and the asymmetry parameter $A_{\rm FB}$ is simply

$$A_{\rm FB} = \frac{\sigma_F - \sigma_B}{\sigma_F + \sigma_B} = \frac{3B}{8A} \tag{3}$$

At low di-lepton invariant masses ($\lesssim$60 GeV), the reaction $q\bar{q} \to \ell^+\ell^-$ is mediated primarily by virtual photons . Around the Z pole it is dominated by the Z boson coupling. In the high mass region it is mediated by a combination of virtual photons and Z bosons. The asymmetry

is very small in the low mass region and near the Z mass peak, and sizable for $M_{\ell\ell}$ =60-80 GeV and $M_{\ell\ell} \geq 110$ GeV.

We use the Collins-Soper frame [17] to reduce the uncertainties due to the transverse momentum of the incoming quarks. In this frame, the angle θ^*_{CS} is defined to be the angle between the lepton momentum and a z axis that bisects the angle between q and $\bar{q}$ directions. The angle θ^*_{CS} is calculated using quantities measured in the lab frame

$$\cos\theta^*_{CS} = \frac{2(P_1^+ P_2^- - P_1^- P_2^+)}{\sqrt{Q^2(Q^2+Q_T^2)}} \tag{4}$$

where Q and Q_T are the four-momentum and the transverse momentum of the di-lepton system, $P_{1,2}$ represent the four momenta of ℓ^+ and ℓ^-, and $P_i^{\pm} = 2^{-1/2}(P_i^0 \pm P_i^3)$. Forward (backward) events are defined by $\cos\theta^*_{CS} > 0$ (< 0).

Without applying any corrections, the uncorrected $A_{\rm FB}$ measurement is distorted from the original parton-level asymmetry because of bin-to-bin migration due to finite resolution of the detector and QED final state radiation (FSR). Moreover, the $A_{\rm FB}$ is further distorted by the detector acceptance and by the unknown quark direction at the LHC. In this paper, we present the uncorrected $A_{\rm FB}$ vs. di-lepton mass and compare it to events generated with the POWHEG Next-to-Leading Order (NLO) generator [19–21] and with detailed GEANT-based CMS simulation and reconstruction [22].

The multivariate analysis of the Drell-Yan process may allow us to study the elementary couplings of fermions to electroweak neutral fields, such as Z/γ^* in the Standard Model, as well as structure functions of the proton. However, as a first illustration of this technique, we take the Standard Model description of electroweak interactions and PDFs in the proton as well-established and allow only the effective electroweak mixing angle $\theta_{\rm eff}$ to be unconstrained, which is the same for both leptons and light quarks with the current precision of this analysis. We illustrate this method with analysis of the $q\bar{q} \to Z/\gamma^* \to \mu^+\mu^-$ process and measure $\sin^2\theta_{\rm eff}$. The choice of $\mu^+\mu^-$, as opposed to e^+e^-, is motivated by the simpler description of detector and background effects in this first study and by the fact that this final state has not been yet studied for $\sin^2\theta_{\rm eff}$ measurements in $q\bar{q}$ interactions. However, we do not expect any limitation in the method for future application to other final states.

We parameterize the Drell-Yan process in proton-proton interactions through elementary $q\bar{q}$ cross-sections and parton functions as follows. The cross-section is parameterized at the leading order, while effects from the next-to-leading-order (NLO) contributions are introduced as corrections extracted from a detailed NLO simulation.

$$\frac{d\sigma_{pp\to l^+l^-X}(Y,s,\cos\theta^*_{CS})}{dY\,ds\,d\cos\theta^*_{CS}} \propto \sum_{q=u,d,s,c,b} \Big[\hat{\sigma}^{\rm even}_{q\bar{q}}(s,\cos^2\theta^*_{CS};\sin^2\theta_{\rm eff}) + D_{q\bar{q}}(s,Y)\times\hat{\sigma}^{\rm odd}_{q\bar{q}}(s,\cos\theta^*_{CS};\sin^2\theta_{\rm eff})\Big]\times F_{q\bar{q}}(s,Y)\,, \tag{5}$$

where $\hat{\sigma}^{\rm even}_{q\bar{q}}$ and $\hat{\sigma}^{\rm odd}_{q\bar{q}}$ are elementary $q\bar{q}$ cross-sections with either even or odd powers of $\cos\theta^*_{CS}$. The parton factor $F_{q\bar{q}}(s,Y)$ arises from the PDFs. It is extracted numerically from the CTEQ6 parameterization [23] and is parameterized analytically in this analysis. The factor $D_{q\bar{q}}(s,Y)$ reflects the fact that the quark direction is unknown and is taken as the boost direction of the system. For $q = u$ or d this factor ranges between 0 and 1 as $|Y|$ changes from 0 up to a maximum value around 4. Information about $\sin^2\theta_{\rm eff}$ is contained in the shape of the 3D distributions in Eq. (5) and enters through elementary couplings of the electroweak bosons and fermions in the process $q\bar{q} \to Z/\gamma^* \to \ell^+\ell^-$.

The expected multivariate distributions in Eq. (5) are further modified by smearing due to detector resolution and FSR and by non-uniform acceptance effects over the phase-space of the observables. All these effects are further taken into account by convolution with a resolution function and by multiplying by an acceptance function. The philosophy of the multivariate likelihood analysis is to first write the phenomenological model of the process and then introduce detector effects into the model to match the observed data. Parameters of the model may either be fixed to the best known values or left free in the fit to be determined from the data. These parameters may include the physical quantities of interest, such as $\sin^2\theta_{\rm eff}$, or a description of the detector effects, such as a correction for the energy scale in the track reconstruction. Systematic uncertainties are estimated from detailed modeling of the process with the POWHEG NLO generator [19–21] and detailed modeling of the detector with GEANT-based CMS simulation and reconstruction [22], as well as from the control sample studies.

The traditional A_{FB} measurement focuses on the asymmetry in the $\cos\theta^*_{\rm CS}$ distribution, as this contains most, but not all, of the kinematic information. The more sophisticated likelihood method utilizes the full triple-differential cross-section to improve the statistical sensitivity to $\sin^2\theta_{\rm eff}$. The improvement is effectively equivalent to a factor of two increase in the data sample.

2 Detector, Data and Monte Carlo Samples

A detailed description of the CMS detector can be found in [22]. The central feature of the CMS detector is a 3.8 T superconducting solenoid of 6 m internal diameter. Within the field volume are the Silicon Pixel and Strip Tracker, the Crystal Electromagnetic Calorimeter (ECAL) and the Brass/Scintillator Hadron Calorimeter (HCAL). In CMS, muons are measured in the pseudorapidity window $|\eta|$ <2.4, with the all-silicon Tracker and the Muon System with detection planes of three technologies, installed outside the solenoid and embedded in the steel return yoke: Drift Tubes (DT), Cathode Strip Chambers (CSC), and Resistive Plate Chambers (RPC) [24]. DTs are used in the barrel ($|\eta|$ <1.2), and CSCs in the endcaps (0.9< $|\eta|$ <2.4), complemented by a system of RPCs covering both regions up to $|\eta|$ <1.6. Electrons are detected in ECAL as energy clusters and as tracks in the Silicon Tracker. ECAL consists of nearly 76 000 lead tungstate crystals which provide coverage in pseudorapidity $|\eta| < 1.479$ in the barrel region (EB) and $1.479 < |\eta| < 3.0$ in the two endcap regions (EE). A preshower detector consisting of two planes of silicon sensors interleaved with a total of 3 X_0 of lead is located in front of the EE.

This analysis uses up to 40 pb^{-1} of proton-proton collision data collected during 2010 by the CMS detector [22] at the LHC with a center of mass energy of 7 TeV. The sample size is reduced by approximately 10% in the analysis of $A_{\rm FB}$ by the requirement of a proper functioning of the ECAL and HCAL detectors in addition to the Muon System and the Tracker.

Signal processes ($Z/\gamma* \to \mu^+\mu^-, e^+e^-$) and the background process $Z \to \tau\tau$ have been simulated on the basis of a Next-to-Leading Order (NLO) calculation using the generator POWHEG [19–21]. Parton showering is simulated using PYTHIA [25]. The NLO PDFs used are CT10 [26]. Background samples of W+jets and $t\bar{t}$ are generated using MadGraph [27], PYTHIA and TAUOLA [28]. Backgrounds from WW, WZ, ZZ, and QCD are generated using PYTHIA. Generated events are processed through the CMS detector simulation and reconstruction. CMS detector simulation is based on Geant 4 [29, 30].

3 Event Reconstruction and Selection

The asymmetry A_{FB} is determined by measuring the mass spectra of di-lepton events in the forward and backward regions separately determined by the polar angle measured in the Collins-Soper frame, $\cos\theta^*_{CS}$. Di-lepton events are selected from events containing two opposite charge, isolated, high p_T leptons. The selection of muons for the likelihood analysis is somewhat different from the selection for the A_{FB} measurement due to special requirements to parameterize the acceptance function and to maximize the information. The di-lepton invariant mass spectrum is analyzed in the range 40–600 GeV, while it is reduced to 60–120 GeV in the likelihood analysis.

3.1 Di-Muon Channel

Muon candidates are selected from an online-trigger-selected sample that contains events with at least one muon found in the volume $|\eta| \leq 2.1$ with a transverse momentum (p_T) of at least 9-15 GeV/c depending on the period of data-taking. For the likelihood analysis, we also use the events found in the volume $|\eta| \leq 2.4$ with $p_T > 3$ GeV/c that are selected by the di-muon trigger.

Offline, muon tracks are first reconstructed independently in the Tracker and the Muon System. Muon candidates are then reconstructed by two different algorithms. The global muon algorithm matches tracks in the Tracker to tracks in the Muon System, and then refits the individual hits in Tracker and Muon System to one overall track. The Tracker muon algorithm extrapolates tracks with $p_T > 0.5$ GeV/c and $p > 2.5$ GeV/c in the Tracker to the Muon System, and a track is taken to be a muon candidate if it matches at least one track segment in the Muon System. Both algorithms take into account energy loss and multiple scattering in the yoke steel of the CMS magnet. High-quality muons are selected by the standard CMS muon identification with requirements on the quantities such as 10 hits in the Tracker, including one in the pixel detector, and at least one hit in the Muon System, hits in at least two muon statitions, and a normalized $\chi^2 < 10$ for the global fit. Muons are required to have a small impact parameter of less than 2 mm measured with respect to the beam spot. Apart from reducing the QCD background, this requirement reduces the cosmic muon background to only a few events. We further require the angle between the two muon tracks to be larger than 2.5 mrad in the laboratory frame, which removes any remaining cosmic ray background and is expected to remove less than one signal event. To isolate single muons from muons overlapping with jets, muons are also required to pass the isolation criteria that uses Tracker and HCAL measurements. The HCAL requirement is not used in the likelihood analysis. The ECAL is not used for muon isolation to reduce the effect from the QED FSR and to maintain more linear efficiency as function of di-lepton mass.

In the A_{FB} measurement, for each muon we require $|\eta| \leq 2.1$ and $p_T > 20$ GeV/c. Below we discuss selection requirement in the likelihood analysis. We relax the two kinematic requirements in the laboratory frame to $|\eta| \leq 2.4$ and $p_T > 18$ and 7 GeV/c for the two muons. However, we introduce additional requirements in the Collins-Soper frame in order to simplify acceptance parameterization: $|\eta^*| < 2.3$ and $p_{T*} > 18$ GeV/c. We also require the di-muon transverse momentum to be less than 25 GeV/c in order to suppress the contribution of events with hard jet radiation. NLO POWHEG simulation predicts that these cuts make the leading-order model a good approximation.

3.2 Di-Electron Channel

Online electron candidates are selected from ECAL L1-triggered events by a high-level trigger requiring an ECAL cluster with minimum E_T between 10 to 17 GeV depending on the

data-taking period. Reconstruction of electrons starts by building superclusters of clusters in the ECAL in order to collect the energy radiated by bremsstrahlung in the Tracker material, following the procedure described in Ref. [31]. A dedicated tracking algorithm is used to better cope with the changes of curvature due to bremsstrahlung. Superclusters are then matched to electron tracks. Electron candidates are required to be in the volumes $|\eta| \leq 1.444$ or $1.566 < |\eta| < 2.500$ with the minimum supercluster E_T of 20 GeV after ECAL energy scale corrections. Electrons from photon conversions are reduced by requiring no missing Tracker hits before the first hit in the reconstructed track matched to the electron and also by rejecting the candidate when a conversion partner track is found close to the electron candidate. High quality electrons are identified by using shower shape variables, and electron candidates are isolated using the Tracker and calorimeters. Electron reconstruction, identification, isolation and trigger efficiency corrections are applied as a function of η and p_T. The corrections are determined using a tag-and-probe method with events from a high purity $Z \to e^+e^-$ sample selected in the 60-120 GeV invariant mass window.

4 Measurement of A_{FB}

For both channels, the main sources of background are $Z \to \tau\tau$ and QCD dijets for the low mass region and $t\bar{t}$ for the high mass region. QCD may be a major background contribution depending on how often a jet fakes an electron and passes the electron ID cuts. We estimate the QCD background in the electron channel using a data-driven method. We assume that same-sign and opposite-sign electron pairs are equally probable since the reconstruction of a charged particle in a jet as a fake electron or positron is equally likely. The QCD background can be estimated by removing the simulated same-sign signal pairs from the same-sign data pairs where simulated same-sign distribution is normalized to the opposite sign distribution. The QCD background in the muon channel is estimated using the simulation and is consistent with the background estimated from the same-sign di-muon events. After applying all selection cuts, the total background is found to be less than 1% in both channels. The estimated background is subtracted for each mass bin for forward and backward events separately.

Figure 1 shows the $\cos\theta^*_{CS}$ distributions in the mass range 40-600 GeV for the di-muon and di-electron channels. The tighter cuts and also the different requirement on $|\eta|$ for the electrons lead to a slightly different shape for the $\cos\theta^*_{CS}$ distribution. Measured and simulated A_{FB} in 11 di-lepton mass bins are shown in Figures 2a and 2b for di-muon and di-electron channels respectively. Here 'simulated' refers to POWHEG-generated events passed through full CMS simulation and reconstruction, with the same selection cuts applied as in data. The mass bin edges are at 40, 50, 60, 76, 86, 91, 96, 106, 120, 150, 200, 600 GeV. We chose to split the Z mass peak because the asymmetry goes through zero near the Z mass peak. The position of the data point within a mass bin is determined by the mean of the di-lepton mass spectrum within the corresponding bin. Statistical errors are calculated using the following formula

$$\Delta A_{FB} = \sqrt{\frac{1 - A_{FB}^2}{N_{obs}}} \tag{6}$$

where N_{obs} is the observed total number of forward and backward events in the corresponding di-lepton bin.

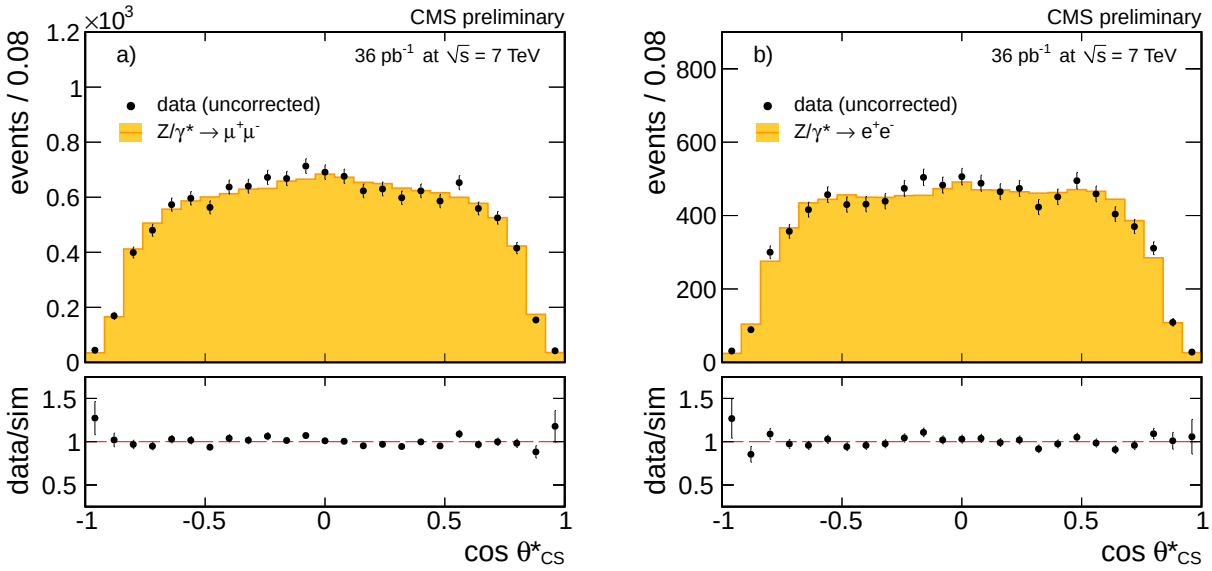

Figure 1: Angle between the lepton momenta and a z axis that bisects the angle between the quark momentum and the anti-quark momentum in the Collins-Soper frame for the muon (a) and the electron (b) channels.

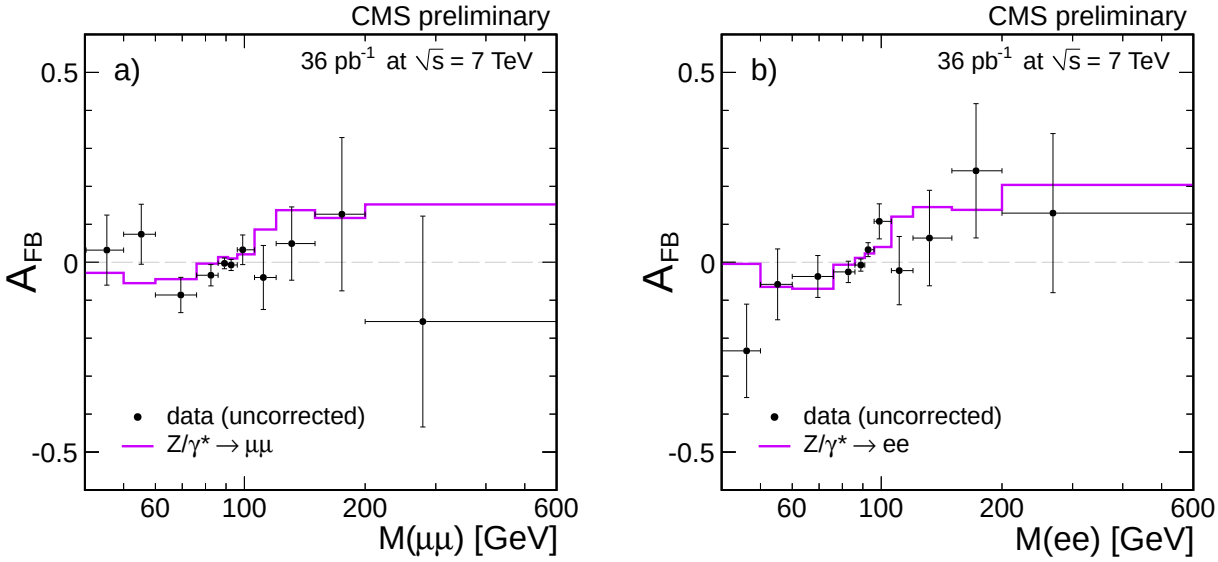

Figure 2: Measured (uncorrected) and estimated A_{FB} in 11 di-muon mass bins in the muon channel (a) and in the electron channel (b).

5 Measurement of $\sin^2\theta_{\rm eff}$

We use an unbinned extended maximum-likelihood (ML) fit describing simultaneously the signal and background yields and the parameters of the $(Y, s, \cos\theta^*_{CS})$ distributions. The likelihood function is written as

$$\mathcal{L} = \exp\left(-n_{\rm sig} - n_{\rm bkg}\right) \prod_i^N \left(n_{\rm sig} \times \mathcal{P}_{\rm sig}(\vec{x}_i;\ \sin^2\theta_W;\ \vec{\xi}) + n_{\rm bkg} \times \mathcal{P}_{\rm bkg}(\vec{x}_i;\ \vec{\xi}) \right) , \qquad (7)$$

where each event candidate i is characterized by a set of three observables $\vec{x}_i = \{Y, s, \cos\theta^*_{CS}\}_i$, $n_{\rm sig}$ is the number of signal events, which includes all intermediate states (γ^*, Z, and their interference), $n_{\rm bkg}$ is the small number of background events, $\mathcal{P}_{\rm type}(\vec{x}_i;\vec{\xi})$ is the probability density function, and $\vec{\xi}$ are the parameters of that function. The number of selected events in the data is $N = 12\,345$ events. The probability density function is defined for signal as

$$\mathcal{P}_{\rm sig}(Y, s, \cos\theta^*_{CS}; \sin^2\theta_W) = \mathcal{G}(Y, s, \cos\theta^*_{CS}) \times \int_{-\infty}^{+\infty} dx\, \mathcal{R}(x)\, \mathcal{P}_{\rm ideal}(Y, s-x, \cos\theta^*_{CS}; \sin^2\theta_W) . \qquad (8)$$

The ideal angular distribution $\mathcal{P}_{\rm ideal}(Y, s, \cos\theta^*_{CS}; \sin^2\theta_W)$ in Eq. (8) is the pp cross-section defined in Eq. (5) and is corrected for detector effects, such as acceptance, resolution, and FSR.

The acceptance function $\mathcal{G}(Y, s, \cos\theta^*_{CS})$ describes the non-uniform reconstruction efficiency across the phase-space of the three observables, which includes effects from online trigger requirements, detector acceptance, reconstruction algorithms, and selection requirements. The most important effect is the loss of particles along the beampipe and the second most important effect is the minimum transverse momentum requirement on the leptons. Otherwise the efficiency across the acceptance range, defined by selection requirements $|\eta^*| < 2.3$, $p_T* > 18$ GeV/c, and $60 < m < 120$ GeV, is close to uniform. The above selection requirements define a sharp boundary in the $(Y, s, \cos\theta^*_{CS})$ space. We model the small deviations from a uniform efficiency within those boundaries with correlated polynomial functions using simulation, where the main effect is a loss of efficiency in the vicinity of the acceptance boundaries. We also allow parameters of the model to be free in the fit to data as a cross-check. We find that the results of analysis are very weakly sensitive to details of efficiency parameterization because it is symmetric with respect to $\cos\theta^*_{CS}$.

The effect of the smearing of the muon track parameters, such as muon momentum and direction, due to detector resolution and FSR is most evident in the invariant mass distribution and is parameterized with the function $\mathcal{R}(x)$ in Eq. (8). In the POWHEG-generated MC samples the FSR is modeled with Pythia and we use an alternative model with PHOTOS for cross-checks. We use the difference of the $\sin^2\theta_{\rm eff}$ fit with an alternative FSR model as a systematic uncertainty due to FSR. The detector resolution effects in muon track reconstruction are dominated by effects of the Silicon Tracker alignment. We perform a realistic simulation of the alignment procedure to model statistical precision in track reconstruction. Potential systematic effects in the procedure, such as χ^2-invariant deformations [32], are studied by making empirical corrections to the track parameters which require the average di-muon invariant mass to be independent of the decay orientation in the detector. Any observed deviation in the fit result is considered as a systematic uncertainty. In order to minimize uncertainties from the energy scale bias in track reconstruction, the reconstructed Z mass is left free in the fit, effectively allowing the energy scale to be determined from the fit to data. We also allow the resolution function parameters to be free in the fit as a cross-check of both detector resolution and FSR effects and find results consistent with the nominal fit.

Table 1: Systematic uncertainties in the measurement of $\sin^2\theta_{\rm eff}$.

source	uncertainty
LO model (ISR)	0.0011
PDFs	0.0015
FSR	0.0018
resolution/alignment	0.0022
fit model	0.0010
background	0.0007
total	0.0036

The background contribution is estimated by MC simulation and cross-checked with data-driven techniques for the QCD background estimates. The total expected background is 36 events, or about 0.3% of the signal size. The background is dominated by the cross-feed from the $q\bar{q} \to Z/\gamma^* \to \tau^+\tau^-$ process (about 50% of the background), QCD (about 25%), and several smaller sources such as $t\bar{t}$, di-boson, and inclusive W production (less than 10% each). The probability density function for background $\mathcal{P}_{\rm bkg}(\vec{x}_i;\ \vec{\xi})$ is parameterized in a similar manner to Eq. (8) with an acceptance range defined by the selection requirements and the distributions within the acceptance boundaries parameterized with empirical polynomial functions. The number of background events $n_{\rm bkg}$ is fixed to the expected value and is varied according to its associated uncertainties. The relative size of the background EWK processes, most importantly $\tau^+\tau^-$, is expected to be reproduced well by simulation, while we assign a 50% uncertainty to the QCD rate. The latter translates into a 0.0007 uncertainty on $\sin^2\theta_{\rm eff}$. As a cross-check, we leave the $n_{\rm bkg}$ unconstrained in the fit and find consistent results.

In order to separate the model uncertainties, such as effects, from NLO and PDFs, from the detector and background effects we perform a test with POWHEG-generated samples using a simplified and fast modeling of detector effects. These detector effect are easily reproducible with custom acceptance and resolution functions. Several samples with different values of $\sin^2\theta_{\rm eff}$ between 0.20 and 0.26 were generated. We find that a noticeable bias is introduced in the analysis without a requirement on the di-muon transverse momentum. However, the requirement that the di-muon transverse momentum be less than 25 GeV/c suppresses the contribution of events with hard jet radiation and reduces the rms of the deviation between $\sin^2\theta_{\rm eff}$ fitted and generated values to 0.0011, which has both statistical and systematic components. We believe this uncertainty can be further reduced by increasing the statistical precision of this test and applying a correction to the measured values should a small bias be present. In a similar manner, we test uncertainties from the assumption of the CTEQ PDF model. Simulation with an alternative PDF model from MSTW-2008 [33] provides fit results consistent within 0.0015.

We test the performance of the fitting procedure with 400 samples, each generated according to the observed number of events. Signal events are used from POWHEG-based CMS detector simulation with an input value of $\sin^2\theta_{\rm eff} = 0.2311$. The number of background events is Poisson-distributed according to expectation. The observed mean of the $\sin^2\theta_{\rm eff}$ fit results is 0.2306 ± 0.0004 and the rms is 0.0078. The former is in good agreement with the generated value and the latter is the most likely expected statistical uncertainty. The distribution $(\sin^2\theta_{\rm eff} - 0.2311)$ normalized by the error is in good agreement with a unit-width Gaussian distribution centered at zero, confirming that the error estimates are correct. From these studies with simulated samples and from the above studies of the acceptance model we assign a conservative systematic error associated with the fit model of 0.0010. A comparison of the MC

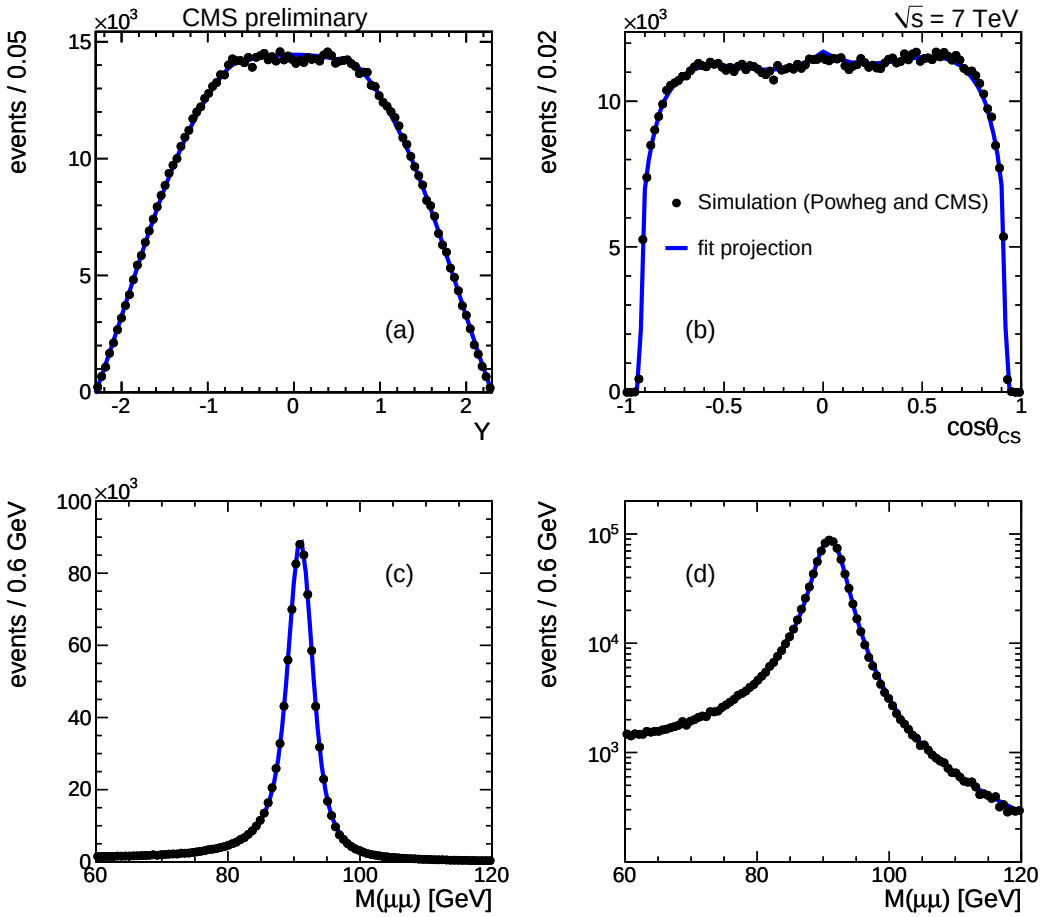

Figure 3: Distribution of Y (a), $\cos\theta^*_{CS}$ (b), m (c and d) in the analysis of $Z \to \mu^+\mu^-$ events from POWHEG-based CMS detector simulation. Smooth lines show projections of the probability density functions.

sample projections and the probability density functions are shown in Fig. 3.

We performed a blind analysis of the data, in which the fit result is not examined until a review of the entire analysis is complete, including all associated systematic uncertainties. The result of the analysis is

$$\sin^2\theta_{\rm eff} = 0.2287 \pm 0.0077(\text{stat.}) \pm 0.0036(\text{syst.})\,, \tag{9}$$

and projections of the data and the probability density functions are shown in Fig. 4. The observed statistical error and the value of likelihood $\mathcal{L}$ are in good agreement with expectation from generated experiments discussed above. We summarize the systematic uncertainties in Table 1. Many of these systematic uncertainties are statistical in nature and may be further reduced with more data and more detailed simulation studies.

6 Conclusions

We have presented the measurement of the forward-backward asymmetry for opposite sign lepton pairs produced via an intermediate $Z/\gamma*$ in pp collisions at $\sqrt{s}$ = 7 TeV. We have also presented the measurement of the effective electroweak mixing angle based on a multivariate likelihood fit which results in a value of $\sin^2\theta_{\rm eff} = 0.2287 \pm 0.0077 \pm 0.0036$. We find both

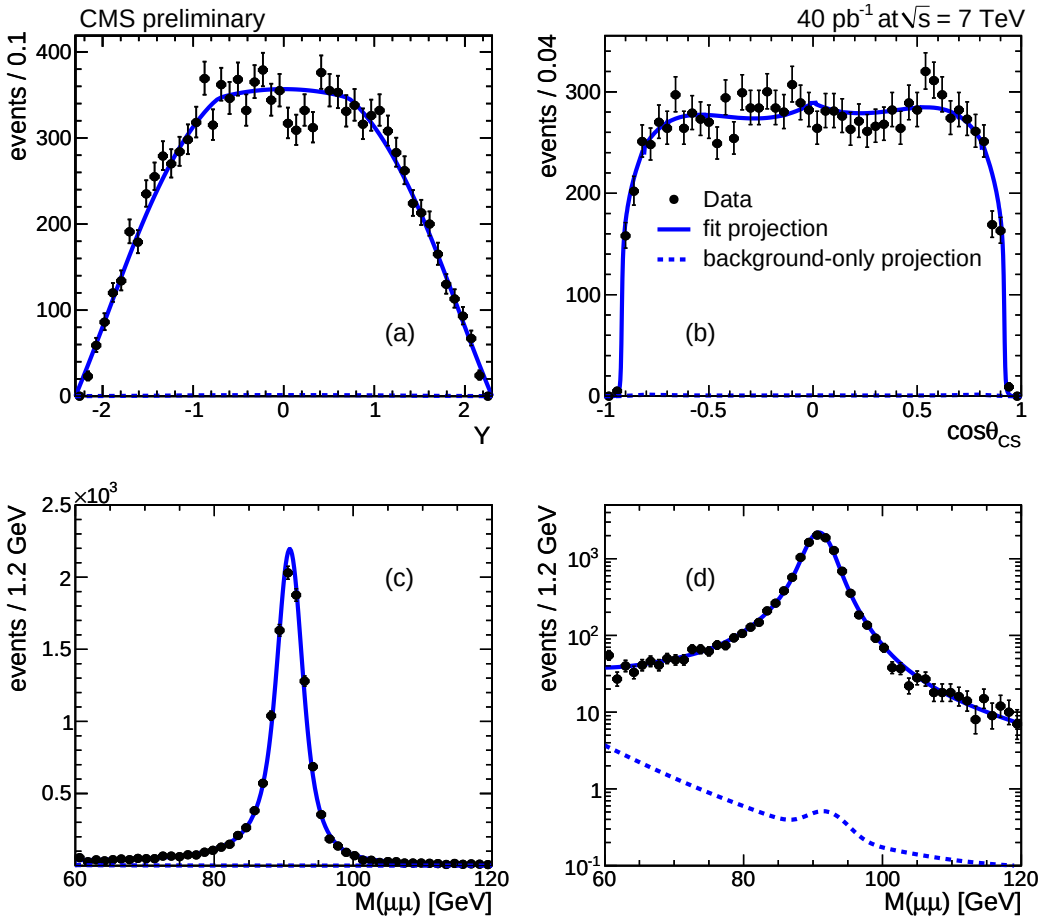

Figure 4: Distribution of Υ (a), $\cos\theta^*_{CS}$ (b), m (c and d) in the analysis of $Z \to \mu^+\mu^-$ events from LHC data. Smooth lines show projections of the probability density functions.

the A_{FB} distributions and the $\sin^2\theta_{\text{eff}}$ measurement to be consistent with the Standard Model predictions within uncertainties.

References

[1] D. London and J. Rosner, "Extra Gauge Bosons in E_6", *Phys. Rev. D* **34** (1986) 1530.

[2] J. Rosner, "Off-Peak Lepton Asymmetries from New Z's", *Phys. Rev. D* **35** (1987) 2244.

[3] M. Cvetic and S. Godfrey, "Electroweak Symmetry Breaking and New Physics at the TeV scale Barklow T L (ed.) et al.", *World Scientific* (1995) 383. arXiv:hep-ph/954216.

[4] J. Rosner, "Forward-backward asymmetries in hadronically produced lepton pairs", *Phys. Rev. D* **54** (1996) 1078. doi:10.1103/PhysRevD.54.1078.

[5] A. Bodek and U. Baur, "Implications of a 300-500 GeV/c^2 Z' boson on $p\bar{p}$ collider data at $\sqrt{s}$=1.8 TeV", *Eur.Phys.J.* **C21** (2001) 607–611. doi:10.1007/s100520100778. arXiv:hep-ph/0102160.

[6] CDF Collaboration, "Search for New Gauge Bosons Decaying into Dileptons in $\bar{p}$p Collisions at $\sqrt{s}$ = 1.8 TeV", *Phys. Rev. Lett.* **79** (1997) 2192–2197. doi:10.1103/PhysRevLett.79.2192. Pillai, M., PhD. Thesis University of Rochester (1996).

[7] F. e. a. Abe, "Limits on Quark-Lepton Compositeness Scales from Dileptons Produced in 1.8 TeV p$\bar{p}$ Collisions", *Phys. Rev. Lett.* **79** (1997) 2198. doi:10.1103/PhysRevLett.79.2198.

[8] D. H., H. J.L., and R. T.G., "Phenomenology of the Randall-Sundrum Gauge Hierarchy Model", *Phys. Rev. Lett.* **84** (2000) 2080–2083. doi:10.1103/PhysRevLett.84.2080.

[9] The D0 Collaboration Collaboration, "Measurement of the Forward-Backward Charge Asymmetry and Extraction of $sin^2\theta_W^{eff}$ in $p\bar{p} \to Z/\gamma^* + X \to e^+e^- + X$ Events Produced at $\sqrt{s} = 1.96$ TeV", *Phys. Rev. Lett.* **101** (Nov, 2008) 191801. doi:10.1103/PhysRevLett.101.191801.

[10] CMS Collaboration, "CMS technical design report, volume II: Physics performance", *J. Phys.* **G34** (2007) 995–1579. doi:10.1088/0954-3899/34/6/S01.

[11] R. Cousins, J. Mumford, and V. Valuev, "Measurement of Forward-Backward Asymmetry of Simulated and Reconstructed Z'$\to \mu^+\mu^-$ Events in CMS", *CMS Note* **2005/022** (2005).

[12] G. Majumder, A. Saha, D. Green et al., "Measurement of the Forward-Backward Asymmetry ($A_F B$) in Z$\to \mu\mu$ events in CMS at $\sqrt{s}$=7 TeV", *CMS Note* **2010/161** (2010).

[13] CMS Collaboration, "Measurement of the Forward-backward in $Z/\gamma* \to \ell^+\ell^-$ Events in CMS at $\sqrt{s}$=7 TeV", *CMS CR Note* **2010/202** (2010).

[14] CMS Collaboration, "Measurement of Forward-backward Asymmetry with Muon Pairs via $Z/\gamma*$ at 7 TeV in CMS", *CMS CR Note* **2010/150** (2010).

[15] CDF Collaboration, "Measurement of the forward-backward charge asymmetry of electron-positron pairs in $p\bar{p}$ collisions at $\sqrt{s} = 1.96$ TeV", *Phys. Rev. D* **71** (Mar, 2005) 052002. doi:10.1103/PhysRevD.71.052002.

[16] H. Yin, "Measurement of the Forward-Backward Charge Asymmetry(A_{FB}) using $p\bar{p} \to Z/\gamma* \to e^+e^-$ events in $\sqrt{S} = 1.96$ TeV",. FERMILAB-THESIS-2010-18.

[17] J. Collins and D. Soper, "Angular Distribution of Dileptons in High-Energy Hadron Collisions", *Phys. Rev. D* **16** (1977) 2219. doi:10.1103/PhysRevD.16.2219.

[18] Y. Gao et al., "Spin determination of single-produced resonances at hadron colliders", *Phys. Rev.* **D81** (2010) 075022, arXiv:1001.3396. doi:10.1103/PhysRevD.81.075022.

[19] P. Nason, "A New Method for Combining NLO QCD with Shower Monte Carlo Algorithms", *JHEP* **11** (2004) 040. doi:10.1088/1126-6708/2004/11/040. arXiv:hep-ph/0409146.

[20] S. Frixione, P. Nason, and C. Oleari, "Matching NLO QCD Computations with Parton Shower Simulations: the POWHEG method", *JHEP* **11** (2007) 070. doi:10.1088/1126-6708/2007/11/070. arXiv:0709.2092.

[21] S. Alioli, P. Nason, C. Oleari et al., "NLO Vector-Boson Production Matched with Shower in POWHEG", *JHEP* **07** (2008) 06. doi:10.1088/1126-6708/2008/07/060. arXiv:0805.4802.

[22] CMS Collaboration, "The CMS experiment at the CERN LHC", *JINST* **0803** (2008) S08004.

[23] F. O. W. T. S. Kretzer, H.L. Lai, "CTEQ6 Parton Distributions with Heavy Quark Mass Effects", *Phys. Rev.* **D 69** (2004) 114005. doi:10.1103/PhysRevD.69.114005.

[24] CMS Collaboration, "CMS MUON Technical Design Report", *CERN/LHCC* **32** (1997).

[25] T. Sjostrand, S. Mrenna, and P. Skands, "PYTHIA 6.4 Physics and Manual", *JHEP* **05** (2006) 026. arXiv:hep-ph/0603175.

[26] H.-L. Lai, M. Guzzi, J. Huston et al., "New Parton Distributions for Collider Physics", (2010). arXiv:1007.2241.

[27] J. Alwall, P. Demin, S. de Visscher et al., "MadGraph/MadEvent v4: The New Web Generation", *JHEP* **09** (2007) 028. doi:10.1088/1126-6708/2007/09/028. arXiv:0706.2334.

[28] N. Davidson, G. Navana, T. Przedzinski et al., "Universal Interface of TAUOLA Technical and Physics Documentation", (2010). arXiv:1002.0543.

[29] J. Sulkimo, M. Takahata, S. Tanaka et al., "Geant 4 – A Simulation Toolkit", *NIM A* **506/3** (2003) 250–303. doi:doi:10.1016/S0168-9002(03)01368-8.

[30] J. Allison, K. Amako, J. Apostolakis et al., "Geant4 developments and applications", *IEEE Transactions on Nuclear Science* **53/1** (2006) 270–278. doi:10.1109/TNS.2006.869826.

[31] S. Baffioni et al., "Electron reconstruction in CMS", *Eur. Phys. J.* **C49** (2007) 1099–1116. doi:10.1140/epjc/s10052-006-0175-5.

[32] CMS Collaboration, "Alignment of the CMS Silicon Tracker during Commissioning with Cosmic Rays", *JINST* **5** (2010) T03009, arXiv:0910.2505. doi:10.1088/1748-0221/5/03/T03009.

[33] A. D. Martin, W. J. Stirling, R. S. Thorne et al., "Parton distributions for the LHC", *Eur. Phys. J.* **C63** (2009) 189–285, arXiv:0901.0002. doi:10.1140/epjc/s10052-009-1072-5.